Supporting Information

Stable Cellulose/Graphene Inks Mediated by Inorganic Base for the Fabrication of Conductive Fibers

Shaoxue Pan,[a] Peng Wang, [b] Peiying Liu,[a] Tianqi Wu,[a] Yicheng Liu,[a] Jianhua Ma *[c] and Hongbin Lu* [a]

a. State Key Laboratory of Molecular Engineering of Polymers, Department of Macromolecular Science, Collaborative Innovation Center of Polymers and Polymer Composites, Fudan University, 2005 Songhu Road, Shanghai 200438, China

b. Institute of Chemical Materials, China Academy of Engineering Physics, Mianyang 621900, China

c. School of Materials Science and Engineering, Xi'an Polytechnic University, Xi'an, Shaanxi 710048, China

Note S1. Molecular Simulation Methodology

All simulations were done with the Large-scale Atomic/Molecular Massively Parallel Simulator (LAMMPS) software package.[1] The molecular structure of graphene was generated using the Make-Graphitics program developed by Sinclair et al.[2,3] The size of the graphene used in the simulation is 60*60 $Å^2$, the C/O ratio is 8.47, the ratio of carboxyl groups to hydroxyl groups in the edge region is 4:1, and the number of hydroxyl groups in the middle region is 3. Since the size of the graphene used in the simulation is much smaller than the graphene in the experiment, in order to balance the C/O ratio and the density of oxygen-containing functional groups at the edge of the graphene, it is reasonable to use a slightly lower C/O ratio. Considering that the size of graphene in the experiment is larger than the length of the cellulose molecular chain, the cellulose molecular chain used in the simulation contains 10 monomers and the length is about 48 Å. Moreover, the effect of LiOH-urea which has been removed from the wet-state fibers has been ignored. First, a simulation box with a size of 90*90*208 $Å^3$ was built using the Packmol program package, containing 2 graphene nanosheets arranged in parallel up and down and 144 cellulose molecular chains distributed between the graphene nanosheets. The cellulose chains in the initial configuration are placed along the x-direction, and the opposite pulling force of 2 Kcal/$Å^2$ is applied at both ends to maintain its orientation, while the movement of the carbon atoms of graphene in the x- and y-directions are limited by a spring potential and only allows movement in the z-direction. Then, the Nose-Hoover algorithm is used to maintain the temperature at 500K, and after several cycles of "decrease-rise-decrease the dielectric

constant", run 4 million steps to slowly reduce the dielectric constant to 1.0. Then, run another 500,000 steps to gradually reduce the temperature to 298K, and then continue to run 500,000 steps to make the system closer to equilibrium. In the final 500,000 steps simulation, the tensile force acting on both ends of the cellulose molecular chain and the spring potential limiting the movement of graphene were canceled to relax the stress generated by the tensile force and spring potential. In equilibrium molecular dynamics, the total simulation time is 100 ns. In the stretching non-equilibrium molecular dynamics simulation, the time step is 0.25 fs, the stretching direction is the x-direction, the engineering tensile strain rate is 10^{10}/s, and the y- and z-directions maintain a pressure of 1.0 atm. To facilitate the analysis of the hydrogen bond energy, all the energy of the system was evaluated by the ReaxFF force field.[4] The visualization of the simulation system was done with VMD 1.9.2 and Ovito 3.0.[5,6]

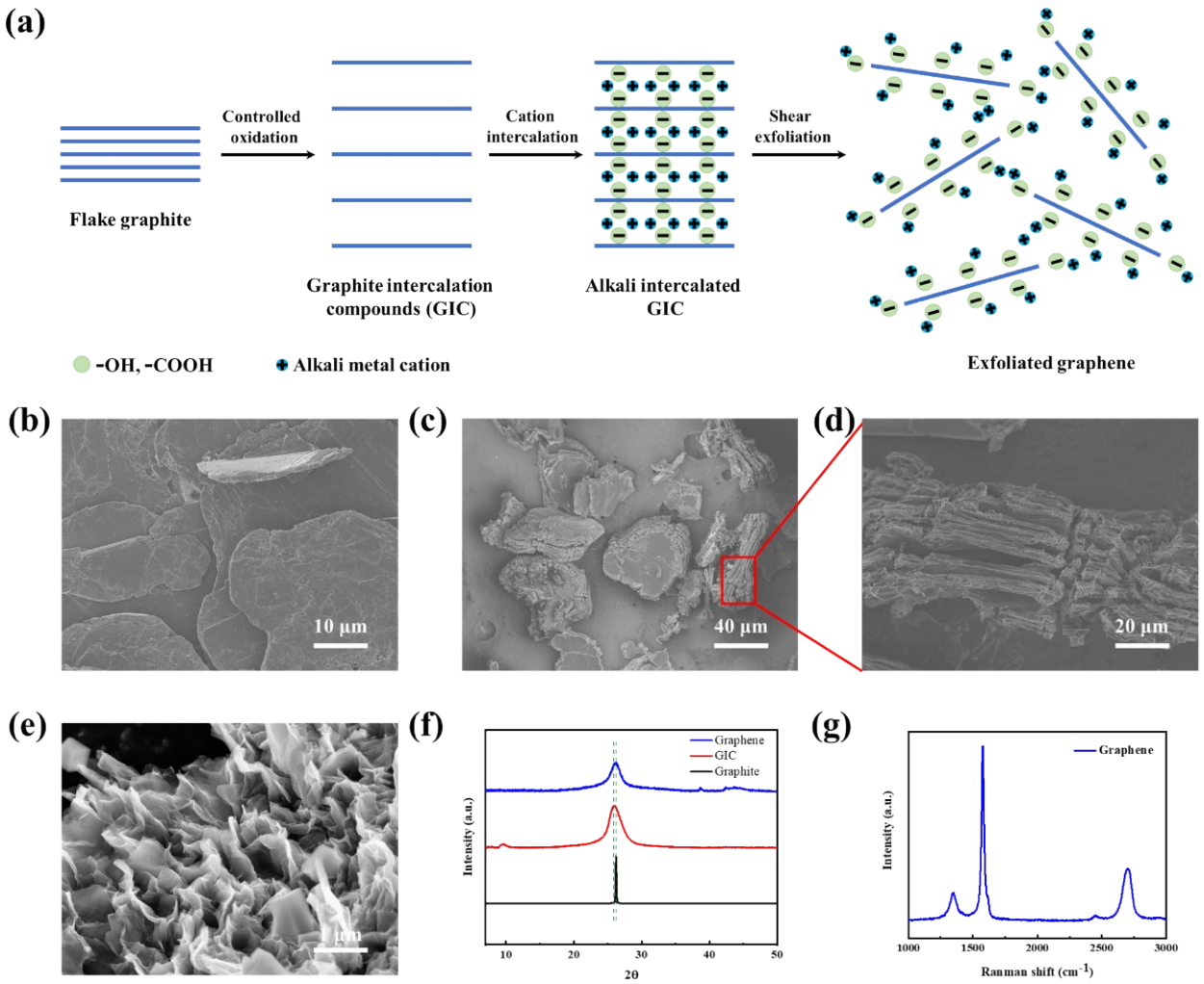

Figure S1. (a) Schematic illustration of the preparation of graphene nanosheets. SEM images of (b) flake graphite, (c, d) graphite intercalation compounds (GIC) and (e) freeze-dried graphene slurry. (f) XRD patterns of flake graphite, graphite intercalation compounds and dry graphene powder. (g) Raman spectra of graphene, showing a low I_D/I_G ratio.

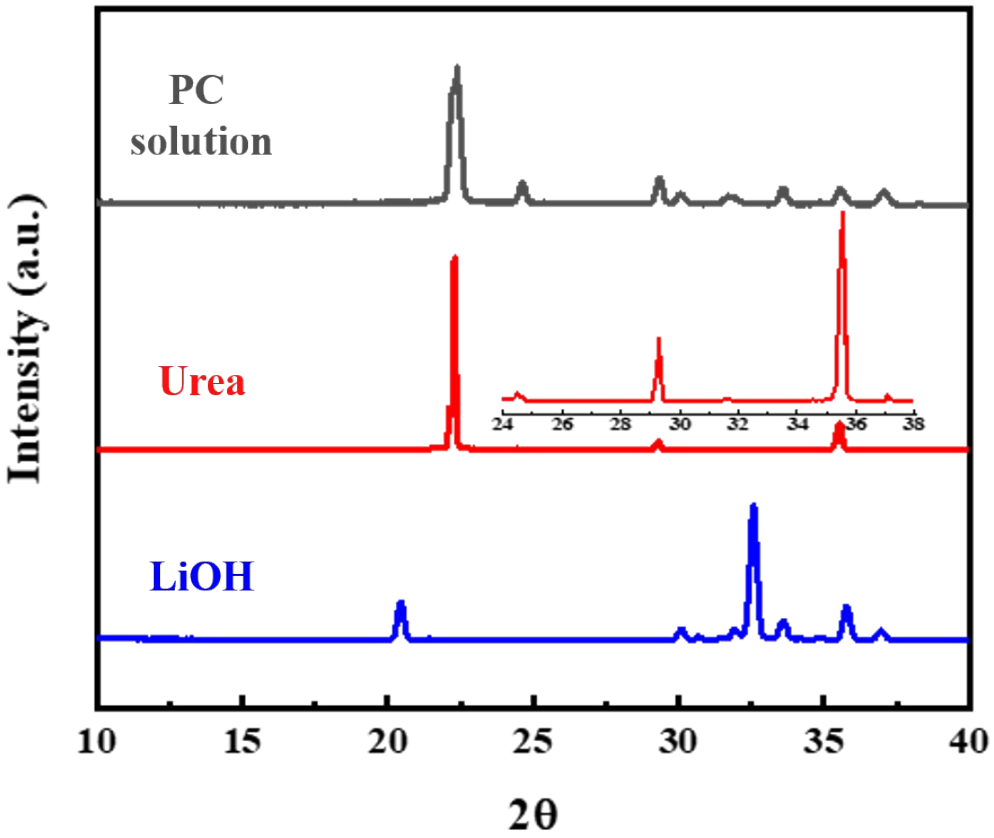

Figure S2. XRD patterns of the freeze-dried PC solution, urea powder and LiOH powder. The disappearance of cellulose crystallization peak indicated that cellulose was dissolved in LiOH-urea solution.[7]

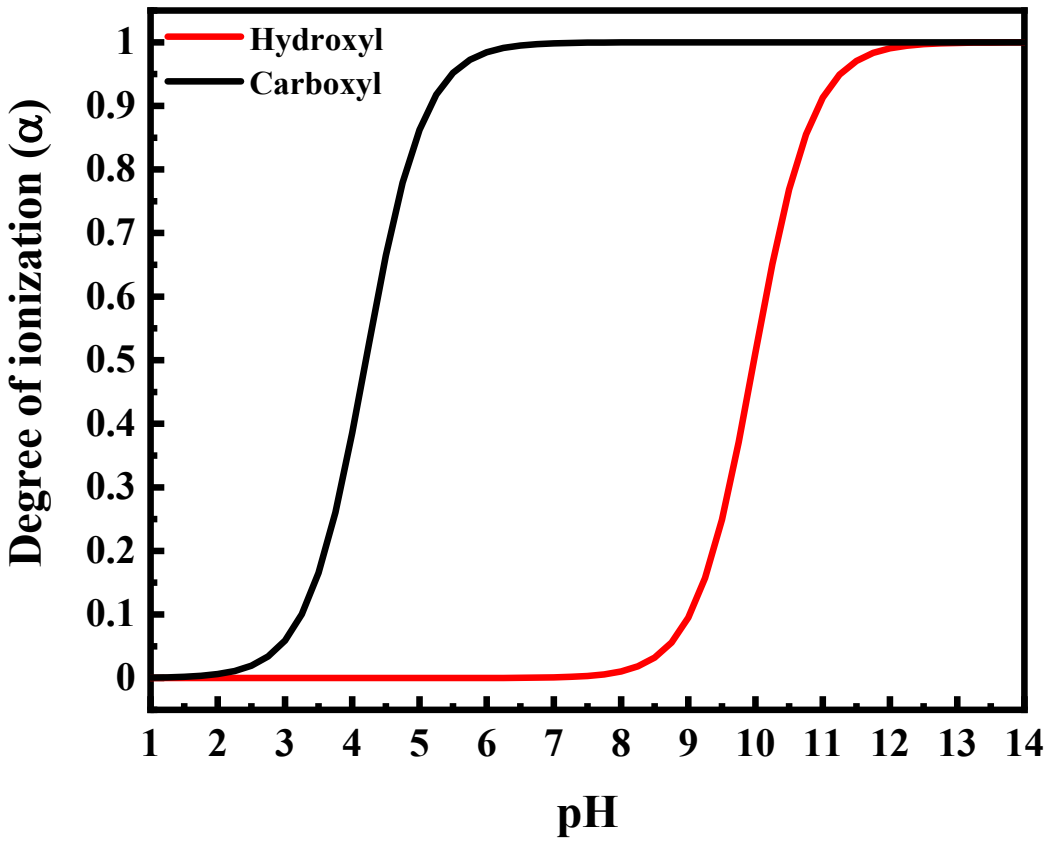

Figure S3. Ionization curve of phenolic hydroxyl groups and carboxyl groups on graphene nanosheets. Degree of ionization (α) = K_a / (K_a + 10^{-pH}). The ionization equilibrium constants (K_a) of benzoic acid and phenol are 6.27*10^-5 and 1.05*10^-10 at 25 ℃ respectively.[8,9] It is generally believed that the only functional groups that can ionize on the surface of graphene are -COOH and -OH.[10] By calculating the degree of ionization (α) of benzoic acid and phenol, the ionization of groups on the surface of graphene can be indirectly reflected. The ionization curve shows that the -COOH groups on the graphene surface were almost completely ionized at pH=7, and the ionization degree of -OH increases from 1% to 99% at the pH range of 8.0~12.0. Therefore, the ionization of graphene surface groups depends on -OH in alkaline

environment, which is consistent with the fact that the graphene prepared at room temperature and low water content is mainly -OH and epoxy groups.[11]

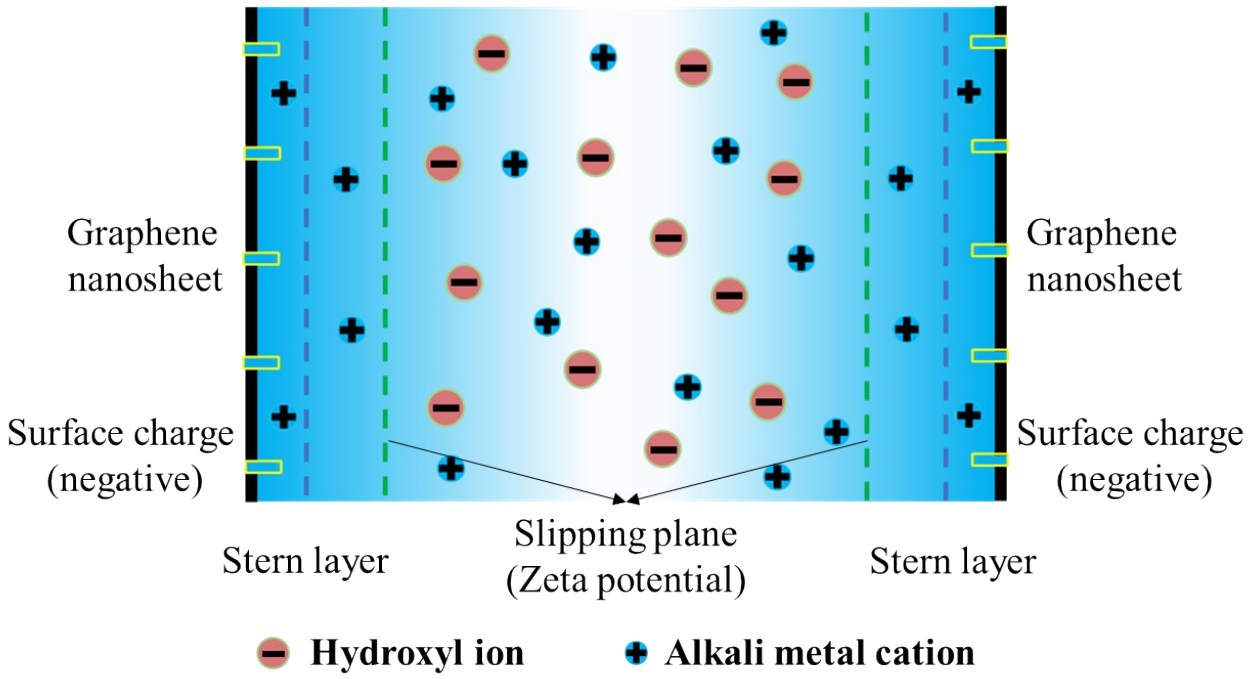

Figure S4. Schematic diagram of electric double layer model of graphene nanosheets in alkaline aqueous solution.[10,12] The phenolic hydroxyl groups ionized under the action of hydroxide ions on the graphene surface carried a negative charge and adsorbed Li-ions in the solution through electrostatic action. The inner region where Li-ions and ionized -OH groups are tightly combined is called the stern layer, and the outer diffusion region where Li-ions are not so tightly absorbed. A boundary abstracted from the diffusion zone is called the slipping plane. In this plane is a stable entity composed of Li-ions and ionized -OH groups, and the formed Li-ions layer will move with the movement of the graphene nanosheets. The zeta potential is the potential from the slipping plane to the bulk solution. When the pH continues to increase, the -OH group has been completely ionized, and the ion concentration in the bulk solution increases,

repelling each other, and more Li-ions will be squeezed into the sliding plane, neutralizing the negative charge, making the absolute value of the zeta potential change small.

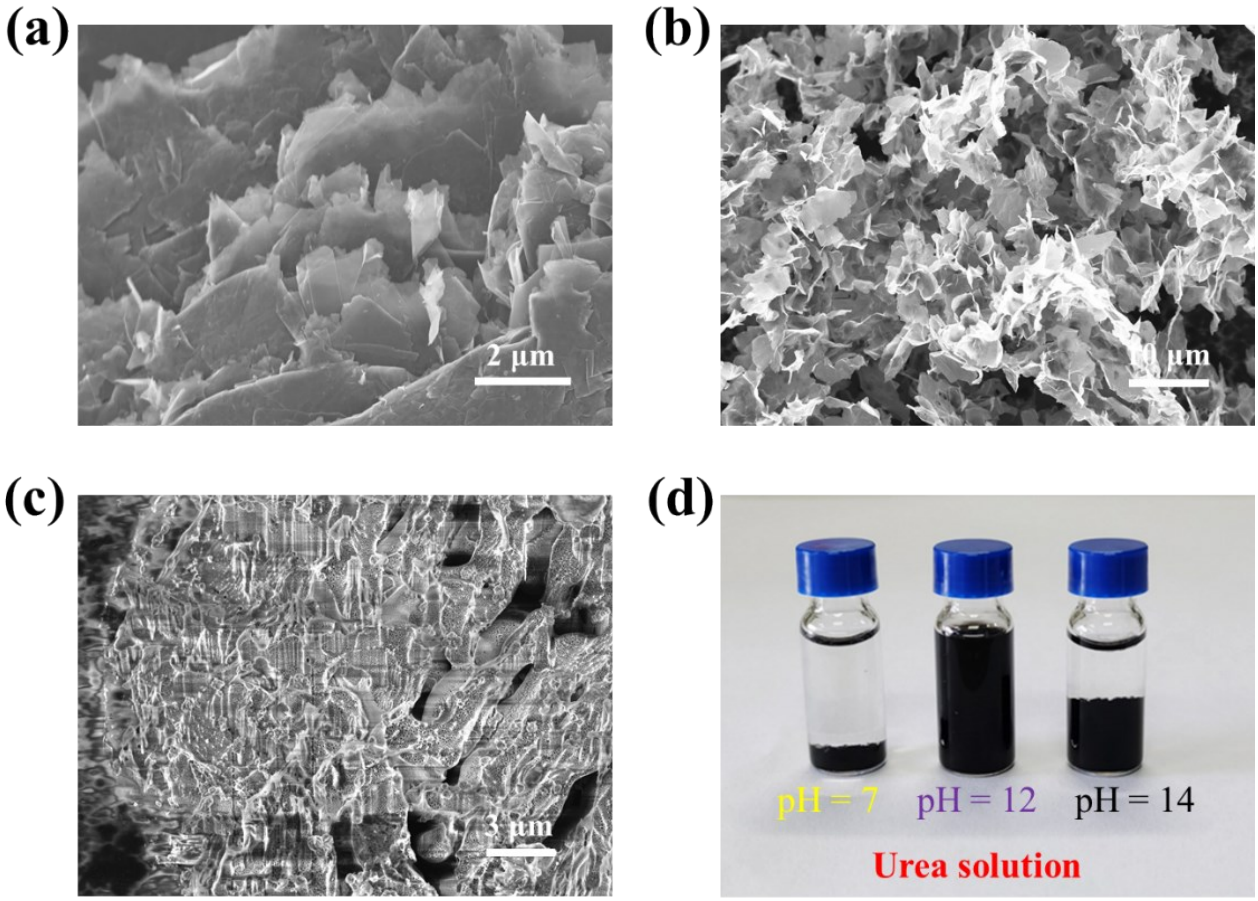

Figure S5. SEM images of graphene with (a) close π-π stacking structure in water (pH = 7), (b) uniformly dispersed structure in LiOH solution (pH = 12) and (c) loosely stacking structure in LiOH-urea solution (pH = 14). (d) Digital images of graphene in urea aqueous solution with different pH.

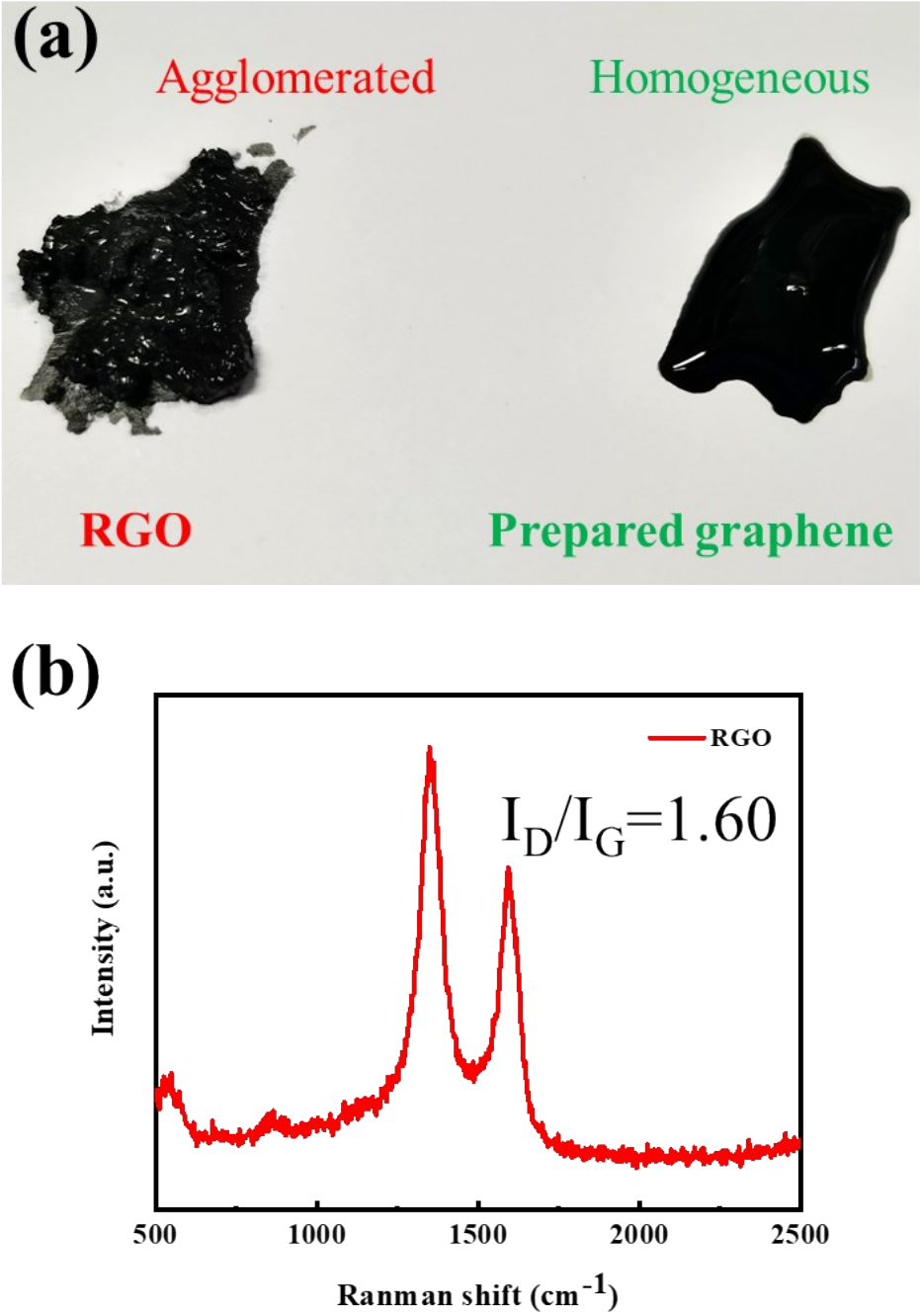

Figure S6. (a) Digital images of cellulose/RGO (left) and CG (right) inks both containing 10 wt% graphene in LiOH-urea aqueous solution. (b) Raman spectra of RGO, showing a high I_D/I_G ratio.

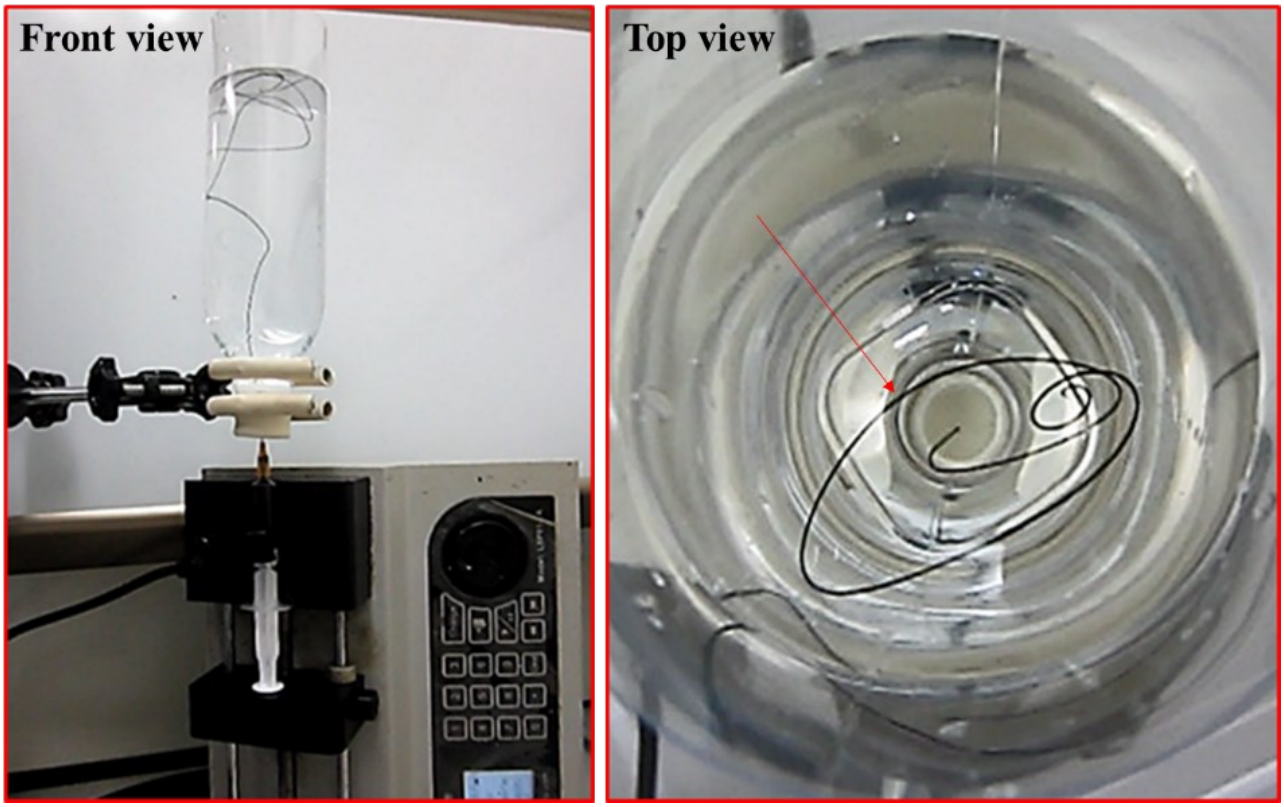

Figure S7. Digital images of assembled wet-spinning device.

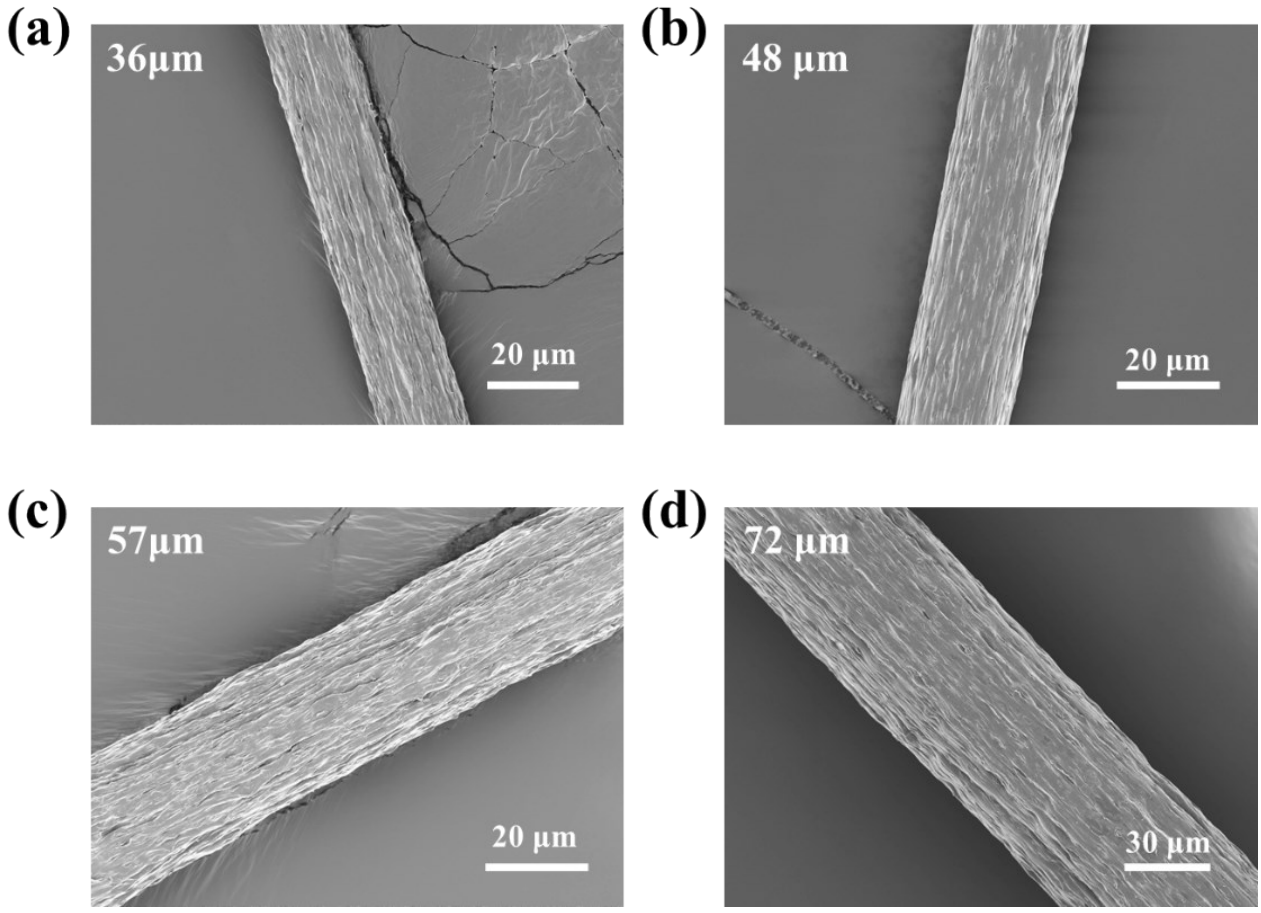

Figure S8. SEM images of the CG fibers with apparent diameters from 36 μm to 72 μm.

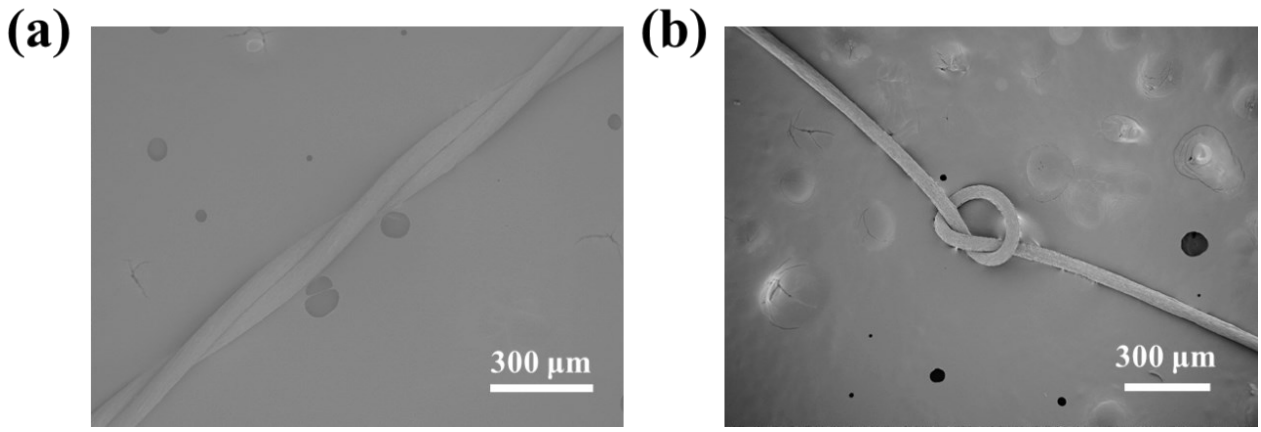

Figure S9. SEM images of the knotted (a) and twisted (b) CG fibers.

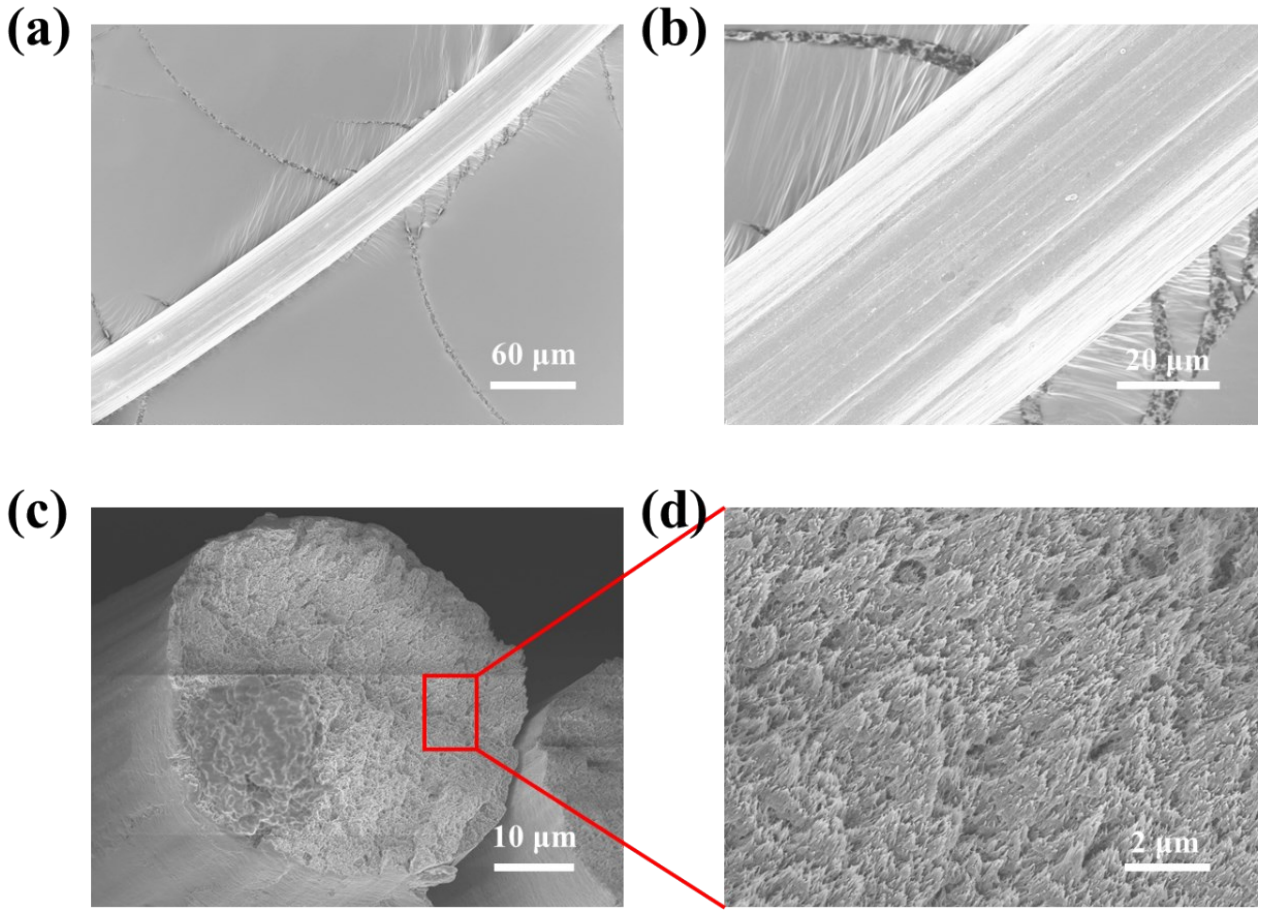

Figure S10. SEM images of the PC fibers with (a, b) smooth surface and (c, d) cross sections.

Table S1. Strength comparison of the present work and the results reported in literature.

Nano-fillers	Cellulose	Solvent involved	Preparation	Fiber type	Tensile strength	Ref.
Graphene	Cotton linter	Alkaline-urea aqueous solution	Wet-spinning	Cellulose/graphene	227.9 ± 6.7 MPa	Our work
MWCNTs/rGO	Cotton pulp	Ionic liquid	Wet-spinning	MWCNTs/rGO/cellulose	2.1 - 5.4 MPa	13
BNNS	Cotton linter	Alkaline-urea aqueous solution	Wet-spinning	RCF/BNNS	~ 140 MPa	14
MXenes	TOCNFs	TEMPO, water	Wet-spinning	TOCNFs/Ti_3C_2	136.5 ± 21.5 MPa	15
GO	NFC	TEMPO, water	Wet-spinning	GO-NFC	274.6 ± 22.4 MPa	16
CNTs	NFC	TEMPO, water	Wet-spinning	CNT-NFC	247 ± 5 MPa	17
CNTs	TCNF	TEMPO, water	Wet-spinning	TCNF/CNT	~ 240 MPa	18
MWCNT	Cellulose	Ionic liquid	Wet-spinning	MWCNT/cellulose	257 ± 9 MPa	19
SWNT	CNF	TEMPO, water	Wet-spinning	CNF/SWNT	~ 472.17 MPa	20
– –	Cotton pulp	CS_2/NaOH	Wet-spinning	Viscose	18.1 cN/tex (~272 MPa)	21
– –	Cotton pulp	CS_2/NaOH	Wet-spinning	Modal	31 cN/tex (~469 MPa)	21
– –	Cotton pulp	NMMO/water	Wet-spinning	Lyocell	31.7 cN/tex (~482 MPa)	21
– –	CNF	(BC)	Wet□drawn	CNF fiber	826 MPa	22

Abbreviations: MWCNTs, multi-walled carbon nanotubes; rGO, reduced graphene oxide; RCF, regenerated cellulose fiber; BNNS, boron nitride nanosheets; TOCNFs, TEMPO (2,2,6,6-tetramethylpiperidine-1-oxylradi-cal)-mediated oxidized cellulose nanofibrils; GO, graphene oxide; NFC, nanofibrillated cellulose; TCNF, Nanocellulose extracted from tunicate; CS2, carbon disulfide; CNF, cellulose nanofibers; NMMO, 4-Methylmorpholine N-oxide; BC; bacterial cellulose

(synthesized by microorganisms, neutralized by NaOH and washed with a large amount of deionized water)

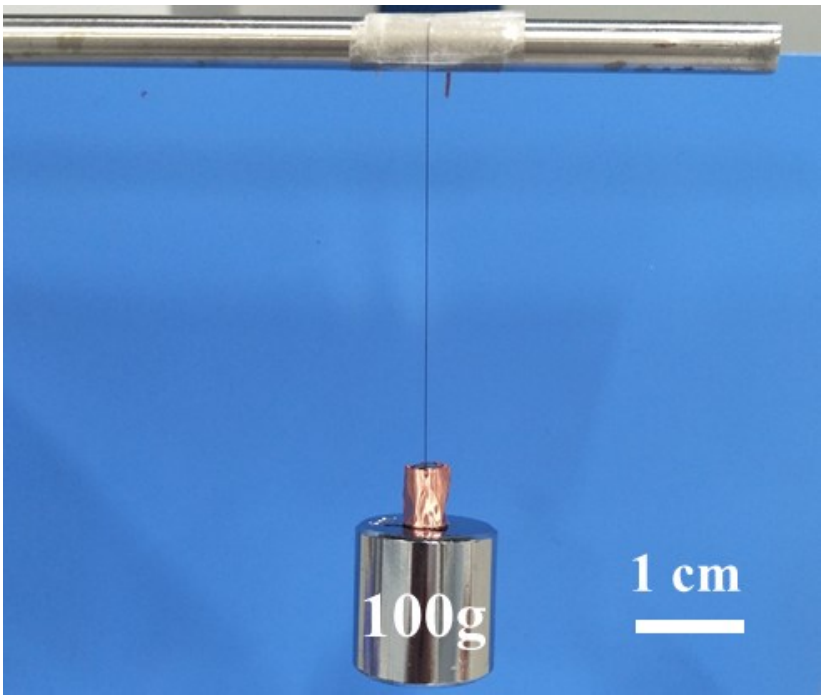

Figure S11. Optical image of a weight weighing 100 g suspended by a 70 μm composite fiber.

Note S2. Calculation of composite fibers density as follows:

$$V_G = \frac{W_G}{W_G + (\rho_G/\rho_C)(1 - W_G)}$$

$$\rho_{CG} = \rho_G V_G + \rho_C V_C$$

where V_G and W_G are the volume and weight fraction of graphene, V_C and ρ_C is the volume fraction and density of the PC matrix, $\rho_{CG}$is the density of CG composites, ρ_G is the density of graphene (~1.06 g/cm^3).[23]

Table S2. Specific tensile strengths of the CG fibers with di□erent graphene contents.

Content (wt%)	Tensile strength (MPa)	Density ($g \cdot cm^{-3}$)	Theoretical density ($g \cdot cm^{-3}$)	Specific strength ($MPa/(g \cdot cm^{-3})$)
0	156.10±6.50	1.575	——	99.11±4.13
2.5	181.01±7.20	1.553	1.556	116.56±4.60
5	227.90±6.74	1.522	1.537	149.74±4.42
10	147.63±5.63	1.474	1.502	100.16±3.80
15	108.10±5.30	1.462	1.468	73.94±3.63

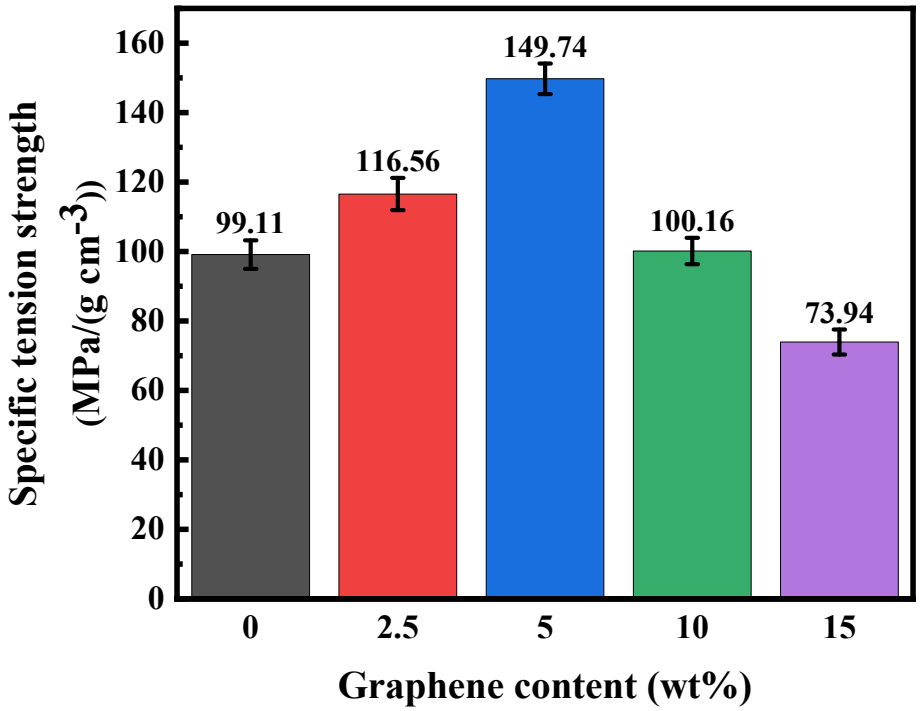

Figure S12. Specific tensile strengths of the CG fibers with di□erent graphene contents.

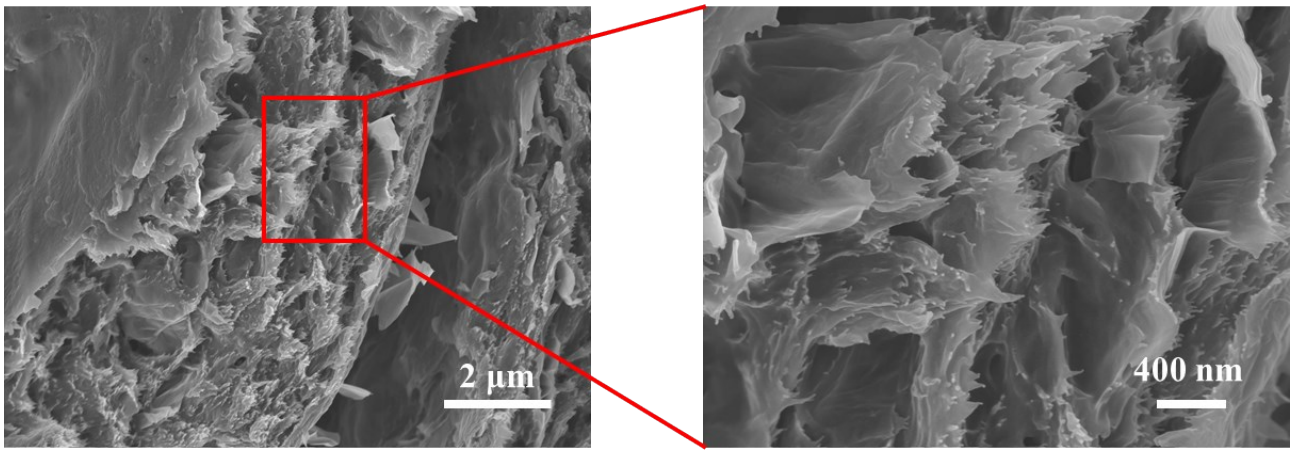

Figure S13. SEM images of the cross-section of a broken composite fiber with ductile fracture characteristics.

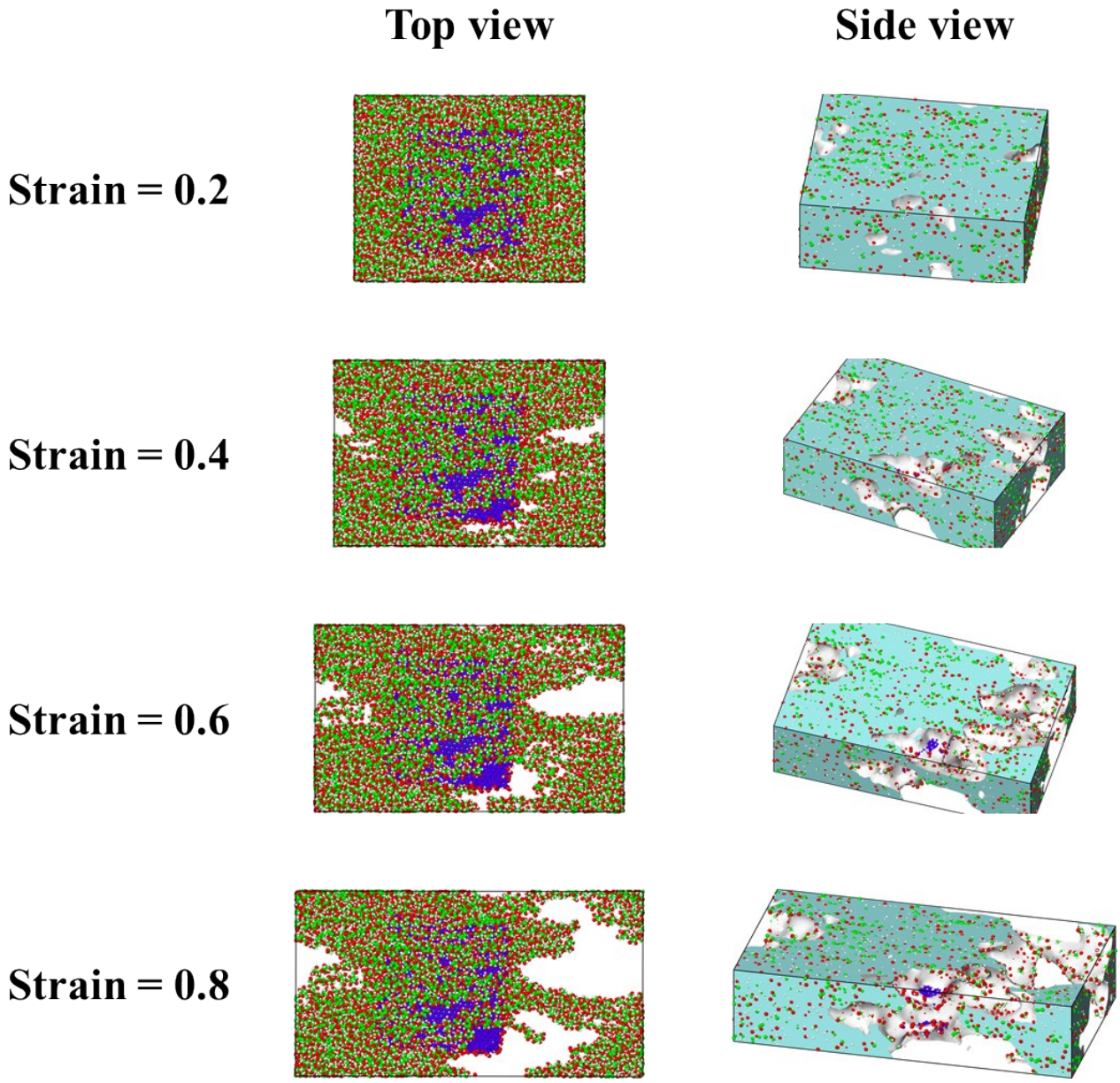

Figure S14. Snapshots of fracture failure of CG system during the simulated stretching process. (green: C; red: O; white: H; blue: carbon atoms of graphene)

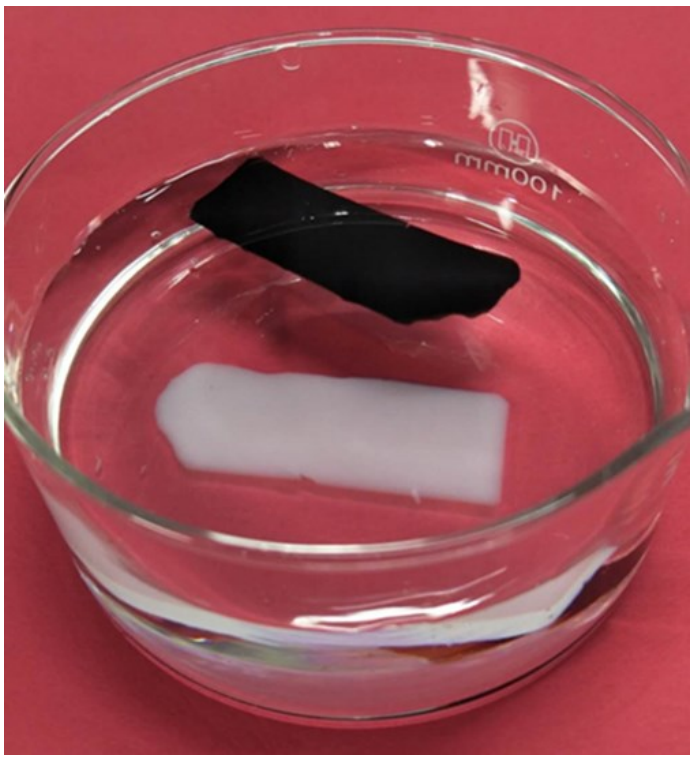

Figure S15. Preparation of the CG and PC films in wet-state.

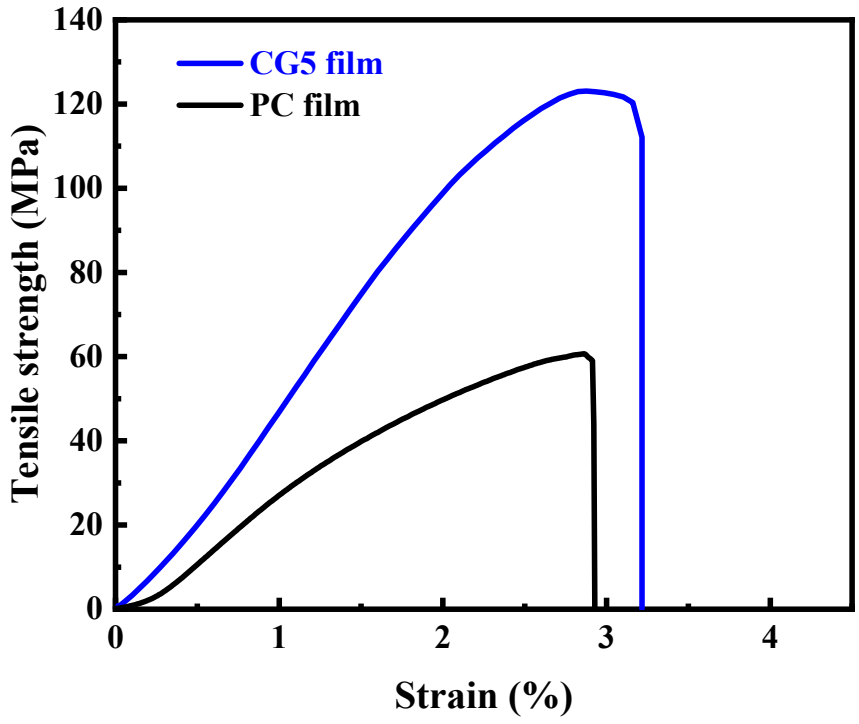

Figure S16. Tensile stress-strain curves of the PC and CG5 films.

Table S3. Comparison of the performance of the samples used to test the electromagnetic shielding performance.

Sample	Tensile strength (MPa)	Strain (%)	Conductivity (S/m)
PC film	60.69±2.37	2.92±0.35	0
PC fiber	156.10±6.50	12.88±0.62	0
CG5 film	123.10±4.85	3.22±0.47	0.82
CG5 fiber	147.63±5.63	11.11±0.59	0.51

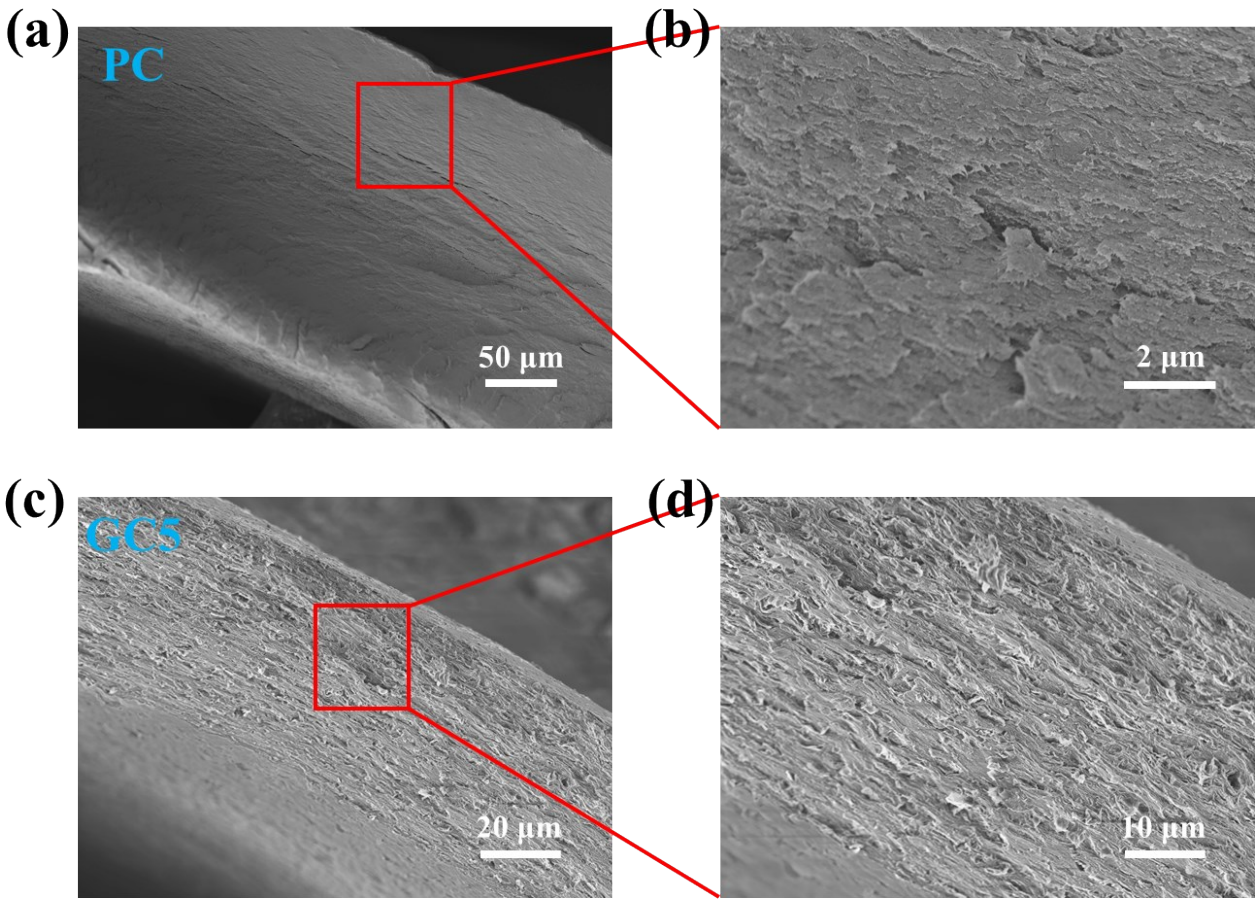

Figure S17. SEM images of the fracture cross-section of PC (a, b) and CG5 films (c, d) in dry-state.

Table S4. Comparison of conductivity of composites with the literature.

Material	Nano-filler	Solvent	Cotent	Conductivity (S/m)	Ref.
Cellulose/Graphene fiber	Graphene	Alkaline-urea aqueous solution	15 wt%	5.11	Our work
GO–NFC hybrid microfiber	GO	Water	50 wt%	~ 0	16
TOCNFs/Ti_3C_2 fiber	MXenes	Water	30 wt%	4.8	15
Hyperbranched polyglycerol/rGO fiber	rGO	DMF	66 wt%	~ 4.88	24
Cellulose/Graphene films	Graphene	DMAC/LiCl solution	1.6 wt%	0.00037	25
Graphene/Silk fibroin film	Graphene	Hexafluoroisopropanol	25 wt%	0.032	26
Graphene/PS composites	Graphene	C_2H_5OH/CH_2Cl_2	30 wt%	1.25	27
Graphene/PVDF film	Graphene	DMF	15 wt%	0.665	28
SWNTS/PNP/PVA fiber	SWNTS/PNP	SDS aqueous solution	SWNTS: 12 wt% PNP: 38 wt%	96.7	29
CNF/SWNT filaments	SWNT	Water	10 wt%	498	20

Abbreviations: SDS, sodium dodecyl sulfate; PNP, permalloy nanoparticle

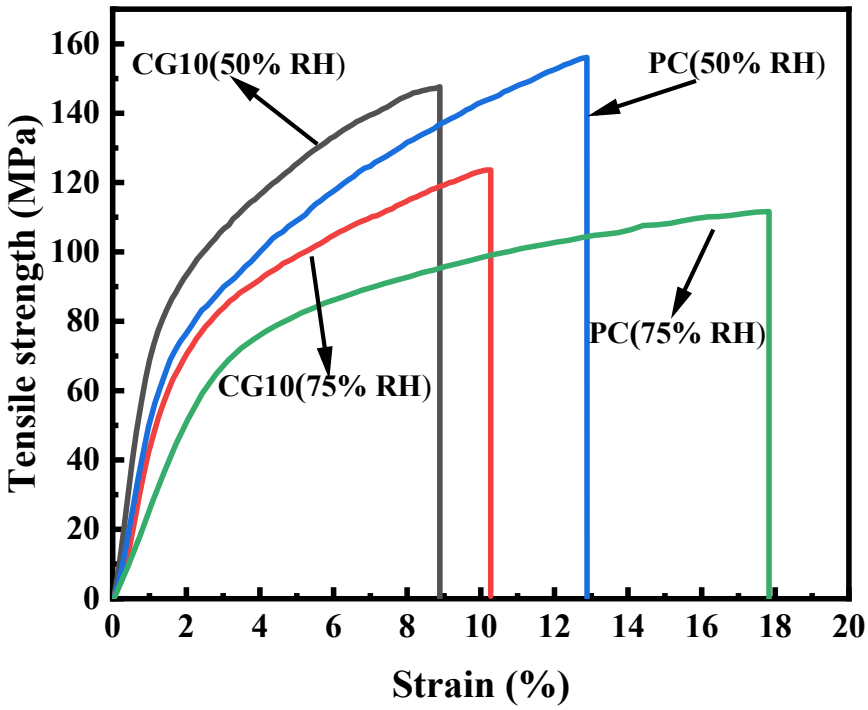

Figure S18. Tensile stress-strain curves of PC and CG10 fibers at 50% and 75% RH.

Table S5. Impact of humidity on mechanical properties of PC and CG10 fibers.

Sample	Tensile strength (MPa)	Strain (%)
PC(50% RH)	156.10±6.50	12.88±0.62
PC(75% RH)	111.63±4.66	17.83±0.86
CG10(50% RH)	147.63±5.63	8.86±0.40
CG10(75% RH)	123.62±5.18	10.27±0.57

Figure S19. A respiratory monitoring sensor based on CG10 fiber; transparent insulating tape was pasted on the copper glue to avoid the interference of human body to the electrical signal.

Table S6. Comparison of EMI between our work with the reported results.

Materials	Fillers	Content	Solvent	Processing	EMI (dB)	Ref.
Cellulose	Graphene	5 wt%	water	Directly mixing	14.6-19.6 @6.5-18 GHz	This work
CNF	RGO	5-30 wt%	water	TEMPO-modified CNF, HI-reduced GO	3-18 @8.2-12.4 GHz	30
CNF	Graphene	12.5-45 wt%	water	Repeated alternated assembly via vacuum filtration	11.5-27.4 @8.2-12.4 GHz	31
Cotton linter	RGO+Fe_3O_4	RGO: 8 wt% Fe_3O_4: 15 wt%	water	Multi-step washing, reduction etc.	32.4-40.1 @8.2-12.4 GHz	32
CNF	TRGO	50 wt%	water	Multi-step process	10-14 @8.2-12.4	33

Abbreviations: TRGO, thermally reduced graphene oxide

Reference

(1) Plimpton, S. Fast Parallel Algorithms for Short-Range Molecular Dynamics. *Journal of Computational Physics* **1995**, *117*, 1-19.

(2) Sinclair, R. C.; Coveney, P. V. Modeling Nanostructure in Graphene Oxide: Inhomogeneity and the Percolation Threshold. *Journal of Chemical Information and Modeling* **2019**, *59*, 2741-2745.

(3) Yang, J.; Shi, G.; Tu, Y.; Fang, H. High Correlation between Oxidation Loci on Graphene Oxide. *Angewandte Chemie International Edition* **2014**, *53*, 10190-10194.

(4) Chenoweth, K.; Van Duin, A. C. T.; Goddard, W. A. ReaxFF Reactive Force Field for Molecular Dynamics Simulations of Hydrocarbon Oxidation. *The Journal of Physical Chemistry A* **2008**, *112*, 1040-1053.

(5) Humphrey, W.; Dalke, A.; Schulten, K. VMD: Visual molecular dynamics. *Journal of Molecular Graphics* **1996**, *14*, 33-38.

(6) Stukowski, A. Visualization and analysis of atomistic simulation data with OVITO–the Open Visualization Tool. *Modelling and Simulation in Materials Science and Engineering* **2009**, *18*, 015012.

(7) Cai, J.; Zhang, L.; Liu, S.; Liu, Y.; Xu, X.; Chen, X.; Chu, B.; Guo, X.; Xu, J.; Cheng, H.; Han, C. C.; Kuga, S. Dynamic Self-Assembly Induced Rapid Dissolution of Cellulose at Low Temperatures. *Macromolecules* **2008**, *41*, 9345-9351.

(8) Fernandez, L. P.; Hepler, L. G. Heats and Entropies of Ionization of Phenol and Some Substituted Phenols. *Journal of the American Chemical Society* **1959**, *81*, 1783-1786.

(9) Read, A. J. Ionization constants of benzoic acid from 25 to 250°C and to 2000 bar. *Journal of Solution Chemistry* **1981**, *10*, 437-450.

(10) Li, D.; Müller, M. B.; Gilje, S.; Kaner, R. B.; Wallace, G. G. Processable aqueous dispersions of graphene nanosheets. *Nature Nanotechnology* **2008**, *3*, 101-105.

(11) Chen, H.; Du, W.; Liu, J.; Qu, L.; Li, C. Efficient room-temperature production of high-quality graphene by introducing removable oxygen functional groups to the precursor. *Chemical Science* **2019**, *10*, 1244-1253.

(12) Ohshima, H. Approximate Expression for the Double-Layer Interaction Energy

between Two Parallel Plates with Constant Surface Charge Density. *Journal of Colloid and Interface Science* **1999**, *212*, 130-134.

(13) Liu, Y. R.; Wang, Y. L.; Nie, Y.; Wang, C. L.; Ji, X. Y.; Zhou, L.; Pan, F. J.; Zhang, S. J., Preparation of MWCNTs-Graphene-Cellulose Fiber with Ionic Liquids. *ACS Sustainable Chemistry & Engineering* **2019**, 7 (24), 20013-20021.

(14) Wu, K.; Yu, L.; Lei, C.; Huang, J.; Liu, D.; Liu, Y.; Xie, Y.; Chen, F.; Fu, Q., Green Production of Regenerated Cellulose/Boron Nitride Nanosheet Textiles for Static and Dynamic Personal Cooling. *ACS Applied Materials & Interfaces* **2019**, 11 (43), 40685-40693.

(15) Cao, W.-T.; Ma, C.; Mao, D.-S.; Zhang, J.; Ma, M.-G.; Chen, F., MXene-Reinforced Cellulose Nanofibril Inks for 3D-Printed Smart Fibres and Textiles. *Adv Funct Mater* **2019**, 29 (51), 1905898.

(16) Li, Y.; Zhu, H.; Zhu, S.; Wan, J.; Liu, Z.; Vaaland, O.; Lacey, S.; Fang, Z.; Dai, H.; Li, T.; Hu, L., Hybridizing wood cellulose and graphene oxide toward high-performance fibers. *NPG Asia Materials* **2015**, 7 (1), e150-e150.

(17) Li, Y.; Zhu, H.; Wang, Y.; Ray, U.; Zhu, S.; Dai, J.; Chen, C.; Fu, K.; Jang, S.-H.; Henderson, D.; Li, T.; Hu, L., Cellulose-Nanofiber-Enabled 3D Printing of a Carbon-Nanotube Microfiber Network. *Small Methods* **2017**, 1 (10), 1700222.

(18) Cho, S.-Y.; Yu, H.; Choi, J.; Kang, H.; Park, S.; Jang, J.-S.; Hong, H.-J.; Kim, I.-D.; Lee, S.-K.; Jeong, H. S.; Jung, H.-T., Continuous Meter-Scale Synthesis of Weavable Tunicate Cellulose/Carbon Nanotube Fibers for High-Performance Wearable Sensors. *ACS Nano* **2019**, 13 (8), 9332-9341.

(19) Rahatekar, S. S.; Rasheed, A.; Jain, R.; Zammarano, M.; Koziol, K. K.; Windle, A. H.; Gilman, J. W.; Kumar, S., Solution spinning of cellulose carbon nanotube composites using room temperature ionic liquids. *Polymer* **2009**, 50 (19), 4577-4583.

(20) Wan, Z.; Chen, C.; Meng, T.; Mojtaba, M.; Teng, Y.; Feng, Q.; Li, D., Multifunctional Wet-Spun Filaments through Robust Nanocellulose Networks Wrapping to Single-Walled Carbon Nanotubes. *ACS Applied Materials & Interfaces* **2019**, 11 (45), 42808-42817.

(21) Kreze, T.; Malej, S., Structural Characteristics of New and Conventional Regenerated Cellulosic Fibers. *Textile Research Journal* **2003**, 73 (8), 675-684.

(22) Wang, S.; Jiang, F.; Xu, X.; Kuang, Y.; Fu, K.; Hitz, E.; Hu, L., Super-Strong, Super-Stiff Macrofibers with Aligned, Long Bacterial Cellulose Nanofibers. *Advanced Materials* **2017**, 29 (35), 1702498.

(23) Rafiee, M. A.; Rafiee, J.; Wang, Z.; Song, H.; Yu, Z.-Z.; Koratkar, N. Enhanced Mechanical Properties of Nanocomposites at Low Graphene Content. *ACS Nano* **2009**, *3*, 3884-3890.

(24) Hu, X.; Xu, Z.; Gao, C., Multifunctional, supramolecular, continuous artificial nacre fibres. *Scientific Reports* **2012,** *2* (1).

(25) Zhang, X. M.; Liu, X. Q.; Zheng, W. G.; Zhu, J., Regenerated cellulose/graphene nanocomposite films prepared in DMAC/LiCl solution. *Carbohydrate Polymers* **2012,** *88* (1), 26-30.

(26) Ling, S.; Wang, Q.; Zhang, D.; Zhang, Y.; Mu, X.; Kaplan, D. L.; Buehler, M. J., Integration of Stiff Graphene and Tough Silk for the Design and Fabrication of

Versatile Electronic Materials. *Adv Funct Mater* **2018,** *28* (9), 1705291.

(27) Yan, D.-X.; Ren, P.-G.; Pang, H.; Fu, Q.; Yang, M.-B.; Li, Z.-M., Efficient electromagnetic interference shielding of lightweight graphene/polystyrene composite. *Journal of Materials Chemistry* **2012,** *22* (36), 18772-18774.

(28) Zhao, B.; Zhao, C.; Li, R.; Hamidinejad, S. M.; Park, C. B., Flexible, Ultrathin, and High-Efficiency Electromagnetic Shielding Properties of Poly(Vinylidene Fluoride)/Carbon Composite Films. *ACS Applied Materials & Interfaces* **2017,** *9* (24), 20873-20884.

(29) Zhou, G.; Wang, Y.-Q.; Byun, J.-H.; Yi, J.-W.; Yoon, S.-S.; Cha, H.-J.; Lee, J.-U.; Oh, Y.; Jung, B.-M.; Moon, H.-J.; Chou, T.-W., High-Strength Single-Walled Carbon Nanotube/Permalloy Nanoparticle/Poly(vinyl alcohol) Multifunctional Nanocomposite Fiber. *ACS Nano* **2015,** *9* (11), 11414-11421.

(30) Yang, W.; Zhao, Z.; Wu, K.; Huang, R.; Liu, T.; Jiang, H.; Chen, F.; Fu, Q., Ultrathin flexible reduced graphene oxide/cellulose nanofiber composite films with strongly anisotropic thermal conductivity and efficient electromagnetic interference shielding. *Journal of Materials Chemistry C* **2017**, 5 (15), 3748-3756.

(31) Li, L.; Ma, Z.; Xu, P.; Zhou, B.; Li, Q.; Ma, J.; He, C.; Feng, Y.; Liu, C., Flexible and alternant-layered cellulose nanofiber/graphene film with superior thermal conductivity and efficient electromagnetic interference shielding. *Composites Part A: Applied Science and Manufacturing* **2020**, 139, 106134.

(32) Chen, Y.; Pötschke, P.; Pionteck, J.; Voit, B.; Qi, H., Multifunctional Cellulose/rGO/Fe3O4 Composite Aerogels for Electromagnetic Interference

Shielding. *ACS Applied Materials & Interfaces* **2020**, 12 (19), 22088-22098.

(33) Han, G.; Ma, Z.; Zhou, B.; He, C.; Wang, B.; Feng, Y.; Ma, J.; Sun, L.; Liu, C., Cellulose-based Ni-decorated graphene magnetic film for electromagnetic interference shielding. *Journal of Colloid and Interface Science* **2021**, 583, 571-578.